PCCP

Accepted Manuscript

This is an *Accepted Manuscript*, which has been through the Royal Society of Chemistry peer review process and has been accepted for publication.

Accepted Manuscripts are published online shortly after acceptance, before technical editing, formatting and proof reading. Using this free service, authors can make their results available to the community, in citable form, before we publish the edited article. We will replace this *Accepted Manuscript* with the edited and formatted *Advance Article* as soon as it is available.

You can find more information about *Accepted Manuscripts* in the Information for Authors.

Please note that technical editing may introduce minor changes to the text and/or graphics, which may alter content. The journal's standard Terms & Conditions and the Ethical guidelines still apply. In no event shall the Royal Society of Chemistry be held responsible for any errors or omissions in this *Accepted Manuscript* or any consequences arising from the use of any information it contains.

ROYAL SOCIETY OF CHEMISTRY

www.rsc.org/pccp

Please do not adjust margins

Journal Name

ARTICLE

Atomic Layer Deposited Tungsten Nitride Thin Films as New Lithium-ion Battery Anode

Received 00th January 20xx,
Accepted 00th January 20xx

DOI: 10.1039/x0xx00000x

www.rsc.org/

Dip K Nandi,[a] Uttam K. Sen,[a] Soumyadeep Sinha,[a] Arpan ~~K.~~ Dhara,[a] Sagar Mitra[a] and Shaibal K Sarkar[a]*

This article demonstrates atomic layer deposition (ALD) of tungsten nitride using tungsten hexacarbonyl [$W(CO)_6$] and ammonia [NH_3] and its use as lithium-ion battery anode. *In-situ* quartz crystal microbalance (QCM), ellipsometry and X-ray reflectivity (XRR) measurements are carried out to confirm the self-limiting behaviour of the deposition. A saturated growth rate of ca. 0.35 Å per ALD cycle is found within a narrow temperature window of 180-195 ^{o}C. *In-situ* Fourier transform infrared (FTIR) vibrational spectroscopy is used to determine the reaction pathways of the surface bound species after each ALD half cycle. The elemental presence and chemical composition is determined by XPS. The as deposited material is found amorphous that crystallized to h-W_2N upon annealing at an elevated temperature under ammonia atmosphere. As deposited materials are found n-type, conducting with average carrier concentration of ca. 10^{20} at room temperature. Electrochemical studies of the as-deposited films opens up the possibility of this material to be used as an anode material in Li-ion battery. The incorporation of MWCNT as a scaffold layer further enhances the electrochemical storage capacity of ALD grown molybdenum nitride (MoNx). An *ex-situ* XRD analysis confirms the conversion based reaction mechanism of the as-grown material with Li under operation.

Introduction

Transition metal nitrides possess significant physical and chemical properties that make it special compared to their analogues transition metal oxides and sulfides. Due to its high electronic and thermal conductivity, it has been used in different purposes such as barrier layer to protect Cu diffusion in semiconductor industries,[1-4] electrocatalyst for hydrogen generation,[5] electrochemical storage materials,[6] coating material for wear and oxidation-resistant tool parts for their high hardness coefficient.[7] Tungsten nitride is also a member of such class of materials and has extensively been used in semiconductor industry as a barrier layer to protect Cu diffusion, catalyst for hydrogen evolution, oxygen reduction reaction[8] and electrochemical capacitor application.[9, 10] A few nanometers of tungsten nitride film can prevent the diffusion of Cu successfully up to as high as 600-700 ^{o}C.

Transition metal binary compounds always have the potential to store lithium through reversible conversion reaction. In the same line, several transition metal nitrides were also tested as anode material for lithium ion batteries mainly because of its highly conducting nature.[11-15] In our earlier work, an ALD deposited molybdenum nitride thin films was successfully used as anode material for lithium ion batteries which explores a new opportunity to use ALD grown transition metal nitride as an active electrode for lithium ion battery application.[16] However, to best of our understanding no such report was found for tungsten nitride.

The overwhelming applications of tungsten nitride are yet to be realized to its potential, due to the inherent difficulties in synthesizing this material. Tungsten nitrides are intrinsically difficult to prepare, as the incorporation of nitrogen into the tungsten lattice is thermodynamically unfavourable at atmospheric pressure.[17] As a reason different high pressure and temperature synthesis process were adopted in literature.[17, 18] Later, tungsten nitride was prepared by adopting a replacement reaction where oxides or sulphides were heated in presence of HN_3 at a high temperature 600 to 900 ^{o}C.[10, 18] Thin films of tungsten nitride were successfully deposited, however limited, by chemical and physical vapor deposition methods.[19-22] Klaus et. al. reported atomic layer deposition (ALD) of tungsten nitride thin films for the first time using WF_6 and NH_3 at a high temperature window of 350-500 ^{o}C.[23] ALD is a well-established deposition technique for depositing thin films with an added advantage of their surface limited reaction chemistry that provides maximum step edge coverage and atomic layer control over the deposition.

[a] Department of Energy Science and Engineering, Indian Institute of Technology Bombay, Powai 400 076, Mumbai, India. Fax:+91 022 2576 4890; Tel: +91 022 2576 4898; E-mail: shaibal.sarkar@iitb.ac.in.

† Footnotes relating to the title and/or authors should appear here.
Electronic Supplementary Information (ESI) available: [details of any supplementary information available should be included here]. See DOI: 10.1039/x0xx00000x

Physical Chemistry Chemical Physics Accepted Manuscript

Please do not adjust margins

Furthermore, to reduce the high deposition temperature the uniformity of N in the film, NH_3 plasma was used along with NH_3 gas itself where the temperature window lies between 200-400 ^{o}C.[24] B_2H_6 was also used with NH_3 eying for lower deposition temperature that brought the ALD temperature window down to 315-375 ^{o}C.[25] Later, the introduction of the metal-organic precursors like (bis-*tert*-butylimido) (bis-dimethylamido) tungsten [$(t\text{BuN})_2(\text{Me}_2\text{N})_2\text{W}$] as a tungsten source not only avoids the production HF but also brings down the down the deposition temperature to 250-350 ^{o}C.[26]
Recently, introduction of $W(CO)_6$ precursor to deposit WO_3 at relatively low temperature was reported.[27] Another transition metal hexacarbonyl$Mo(CO)_6$ was also explored as an potential precursor to deposit MoO_3 as well as Co doped MoO_3.[28, 29] Recently, we have reported the ALD of MoN_x and MoS_2 using $Mo(CO)_6$ as a molybdenum source to show the versatility of the hexacarbonyl precursor towards ALD.[16, 30] This leads us towards the synthesis of tungsten nitride using $W(CO)_6$ as a source for the tungsten. The low temperature window for deposition will obviously enhance the applicability of a material especially related to IC industry and polymer based applications.
Here, we report an ALD chemistry to deposit tungsten nitride using tungsten hexacarbonyl and ammonia. Growth study is performed with *in-situ* quartz crystal microbalance (QCM), *ex-situ*ellipsometry and X-ray reflectivity (XRR) measurements. *In-situ* Fourier transform infrared spectroscopy (FTIR) helps to investigate the surface bound species after each individual ALD half-cycle. The film compositions, crystallinity, and electrical properties are also investigated with the help of X-ray photoelectron spectroscopy (XPS), X-ray diffraction (XRD) and temperature dependent Hall measurements.
The electrochemical activity of as deposited sample was tested against lithium. Similar to other transition metal nitrides, WN_x can react with metallic lithium and produces W nanoparticles and Li_3N. $WN_x$was found to be electrochemically active with excellent cyclic stability. To increase the mass loading of WN_x, surface area of the electrode was increase by introducing a scaffold layer. MWCNT deposited surface was used to grow WN_x. The resultant assembly was tested against lithium and results obtained from this assembly were promising.

Experimental Section

Film Preparation and characterization

Atomic layer deposition of tungsten nitride films were carried out in a custom built viscous flow reactor equipped with capacitance manometer for pressure transient measurements and computer controlled pneumatic valves for controlled reactant dosing. The complete operation was continuously monitored and controlled by computer interfaced with LabView. The base pressure of the reactor was maintained to ca. 1 torr by throttling of ca. 200 sccm of ultra-high purity N_2 gas that was pumped out continuously by rotary pump. The reactants $W(CO)_6$ and NH_3 were kept in room temperature but fed to the reactor through differential heating, using ultra high purity N_2 as carrier gas. For $W(CO)_6$,nitrogen gas was fed through an overhead assembly.
To study the growth of the film, *in-situ* quartz crystal microbalance (QCM) (Inficon) containing a 6MHz AT cut quartz crystal was used. It measures the mass gain during each half cycle during the film growth with a mass resolution of ca. 1ng cm^{-2} under steady state condition. *In-situ* FTIR measurements were performed in a different ALD chamber, similarly equipped as previous to investigate the surface bound chemical species after each half of the ALD reaction under steady state growth condition. Infrared beam was fed to the chamber through ZnSe windows and recorded under absorbance mode. We used liquid nitrogen cooled MCT detector with Bruker Vertex-70 FTIR spectrometer for the measurements. For FTIR measurements KBr palettes were used as substrate that is initially quoted with ALD grown Al_2O_3. X-ray diffraction (XRD) and X-ray reflectivity (XRR) characterizations were performed with Bruker D8-Advance diffractometer equipped with Cu Kα cathode that emits X-ray at 1.54Å. For diffraction measurements films were deposited on microscopic glass substrate while for reflectivity experiments films were grown on single sided polished (111) Si wafers to minimize the interfacial roughness. Experimentally obtained XRR data were fitted with Parratt32 software to obtain the film thickness, roughness and electron density. Furthermore, all thickness measurements were verified with spectroscopic ellipsometry (Sentech) measurements over a wavelength range of 350-850 nm at an incident angle of 70°, performed on the same or similar samples.
X-ray diffraction (XRD) spectroscopy was carried out in RigakuSmartlab X-ray diffractometer equipped with a Cu-K_{α} source to know the crystalline nature of the as-deposited as well as annealed films. Films were grown on amorphous microscopic glass substrates for XRD analysis to avoid any unwanted XRD peak caused by the substrate. Elemental and compositional analyses were performed on Thermo VG Scientific X-ray photoelectron spectrometer (MultiLab) equipped with Al-K_{α} source (1486.6 eV). Peak fittings and analyses were executed using XPS peak 4.1 software. Before any analysis peak positions were adjusted with respect to reference C-1s peak at 284.6 eV. Surface morphology and RMS roughness was studied using VeecoNanoScope IV MultiMode atomic force microscopy (AFM) under semi-contact mode of operation. High resolution transmission electron microscopy (HR-TEM) was carried out in JEOL-2100F to get a small area electron diffraction (SAED) pattern and the HR-TEM images of the lattice array of the annealed film. Temperature dependent Hall measurements were carried out in Ecopia HMS 5000 using four probe Van der Pauw method. Films were deposited on microscopic glass substrates having a dimension of 0.5 cm x 0.5 cm for Hall measurements. Current-voltage (I-V) of the deposited film was measured using Kithley 2400.

Experimental details for electrochemical study

WN_x films were directly deposited on stainless still (SS) coin having a diameter of 1.54 cm. Film of 1500 ALD cycles under

Physical Chemistry Chemical Physics Accepted Manuscript

This journal is © The Royal Society of Chemistry 20xx

self-saturated conditions were prepared for all the electrochemical characterizations. WN_x films were also deposited on pre-treated multi-walled carbon nanotube (MWCNT) that was coated uniformly on SS coin by drop-casting method. Both the bare films and the films on MWCNT were grown under same conditions of ALD reaction to get a comparative study between them.

All the electrochemical characterizations were done in 2032 coin cells in half cell assembly i.e. against lithium. A cell configuration of Li/Electrolyte/WN_x was assembled inside an argon-filled glove box (Lab Star, Mbraun, Germany) with moisture and oxygen concentrations level of ~ 1 ppm. WN_x deposited on stainless steel substrate and CNT deposited stainless steel substrate was directly used as an active electrode without any further treatment. Lithium foil was used as counter electrode which also serves as a reference electrode. 1 M $LiPF_6$ solution in EC/DMC (1:1 wt/wt) (LP-30, Merck, Germany) was used as electrolyte for all electrochemical measurements presented here. A porous separator made of borosilicate glass microfiber filters (Whatman) was used to soak the electrolyte and separate the two electrodes.

Cyclic voltammetry (CV) measurements were carried out with Bio-logic VMP-3, France, while the charge-discharge measurements were performed in BT-2000 test station, Arbin Instruments, USA. CV measurements were performed with in the voltage range of 0.1 - 3.0 V vs. Li/Li^+ at a scan rate of 0.2 mV s^{-1} while the charge discharge performance was scanned from 0.1 V to 2.5 V vs. Li/Li^+ at a current density of 50 µA cm^{-2}. All the electrochemical measurements were taken at a constant temperature of 20°C.

Results and Discussion

ALD of tungsten nitride films were performed with the pulsing condition of mx1-15-nx1-15. Here, m and n are the number of pulses of $W(CO)_6$ and NH_3 doses respectively. Purging time of 15 seconds was used after both the precursor dosing for all experiments here. *In-situ* QCM was used to study the growth rate within the temperature range 170-220 ^{o}C. No deposition was found below 170 ^{o}C while the QCM stability was always a concern beyond 225 ^{o}C. Figure 1a shows the growth rate of the material with the increasing temperature with 1-15-1-15 pulsing. The change in resonance frequency of QCM after each precursor dosage was converted to its corresponding mass by using the Sauerbrey's equation. Thus the mass gain in one complete cycle enabled us to determine the growth rate of the film considering its density as 9.5 gm cm^{-3} as measured by the XRR, discussed later. It is clearly depicted from the figure that a persistent growth rate of ca. 0.08 Å/cycle was achieved within the temperature between 180-195 ^{o}C. This constant growth rate regime is the ALD window which is so far the lowest tungsten nitride ALD. Deposition rate went higher with the temperature beyond 195 ^{o}C indicating a deposition mechanism due to the decomposition of the $W(CO)_6$. Lower growth rate below the ALD temperature window reflects the thermodynamic limitation of the underlying ALD reaction. Hence, further experiments were performed within this ALD temperature window.

Figure 1b shows a couple of representative ALD cycles measured with QCM at 190 ^{o}C. The pressure transients are also shown along with this figure in secondary Y-axis. As expected, a considerable mass increase was noted upon $W(CO)_6$ dosage. We also note a slight change, but highly consistent, in the mass of ca. 1 ng cm^{-2} was noted after NH_3 dose. The total change in the mass upon completion of a one ALD cycle was found to be ca. 7.6 ng cm^{-2} which corresponds to a growth rate of ca. 0.08 Å/cycle, considering the density of the film as 9.5 g cm^{-3}. The growth per individual ALD cycle was found to be consistent.

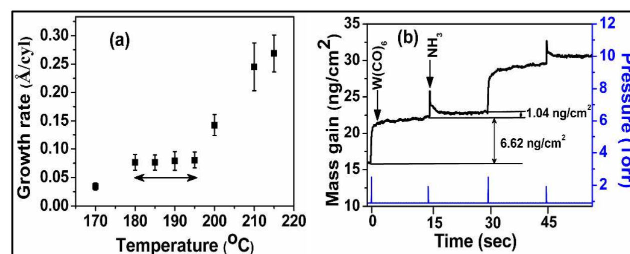

Fig. 1 (a) Temperature window for the ALD deposited WNx as observed by QCM study and (b) mass gain in each half cycle and its corresponding precursor pressure.

The self-limiting behaviour was examined to validate the ALD mechanism. Here, the film deposition was monitored by QCM with increased number of reactant doses at 190 ^{o}C. Figure 2a shows the growth rate versus the reactant $W(CO)_6$ dosages. The measured growth rate from QCM was simultaneously verified by XRR and Ellipsometry measurements. For XRR and Ellipsometry measurements, films were deposited on Si substrate with native SiO_2. From the figure it is clearly depicted that the growth rate eventually levels off beyond three to four consecutive pulses of $W(CO)_6$, corresponding to the total exposure of ca. 7.5 x 10^5 L, yielding to a self-saturated growth rate of ca. 0.35 Å per ALD cycle. On the other hand, the self-limiting behaviour with respect to NH3 exposure was observed only after a single dose of it (2 L). Any further increase in dosages beyond this condition never result any increase in growth rate which strictly indicate a monolayer growth without any polymerization of self-decomposition.

Figure 2b shows the thickness of the ALD grown tungsten nitride films with increasing number of ALD cycles under the saturated pulsing condition, (4x1, 15, 1, 15). The thickness measurements were performed with the ellipsometry. Here the films were deposited on polished Si wafer. It can be clearly seen that the thickness increases linearly with the number of ALD cycles except for a very short incubation period at beginning less than 100 ALD cycles. The average growth rate of the film was found to be ca. 0.36 Å per ALD cycle that was similar as found from the QCM measurements in figure 2a.

Physical Chemistry Chemical Physics Accepted Manuscript

Please do not adjust margins

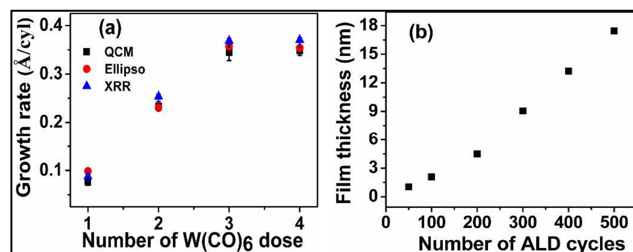

Fig. 2 (a) Growth rate measured by QCM, XRR and ellipsometry with increase number of W(CO)6 dose and (b) thickness of the deposited film with increasing ALD cycles measured by ellipsometry.

In-situ FTIR study was performed to understand the surface species after each half of the ALD reaction. The difference FTIR spectra can be obtained by subtracting present spectra from its earlier one. Basically it considers the earlier spectra as a base line and in such FTIR spectra a positive absorbance peak eventually indicates the presence of a particular species while a negative absorbance peak confirms the absence of the same surface species. Figure 3a and 3b shows the appearance and disappearance of the metal centered carbonyl (W-C=O) IR stretch at 1997 cm^{-1} for first four ALD cycles respectively after the dosing of $W(CO)_6$ and NH_3 which is in good agreement with the CO vibrational stretching mode in gas phase.[31] While the appearance of carbonyl peak after $W(CO)_6$ dose confirmed the presence of $W(CO)_x^*$ after the first half reaction, the absence of the W-C=O stretch after NH_3 dosing meant the removal of $(CO)_x^*$ from the surface. Similar flip-flop nature due to the presence and absence of $–NH_2^*$ surface species at 945 cm^{-1} and 955 cm^{-1} is shown in figure 4a and 4b which we have observed in our earlier work.[16] While figure 4a shows the positive absorbance peak indicating the presence of $–NH_2^*$ after the NH_3 dosing, the negative absorbance peaks of the same after $W(CO)_6$ dosing proves the complete removal of the $–NH_2^*$ from the surface by a $W(CO)_x^*$ surface species. Thus the possible half reactions can easily be predicted from the FTIR study as written below

$W(CO)_x^* + NH_3 \rightarrow W\text{-}NH_2^* + H_2 + CO$ (1)

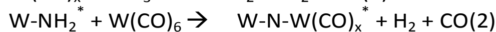
$W\text{-}NH_2^* + W(CO)_6 \rightarrow W\text{-}N\text{-}W(CO)_x^* + H_2 + CO$ (2)

Thus a repeated combination of the above two half reactions under 121212…. Format built the desired material.

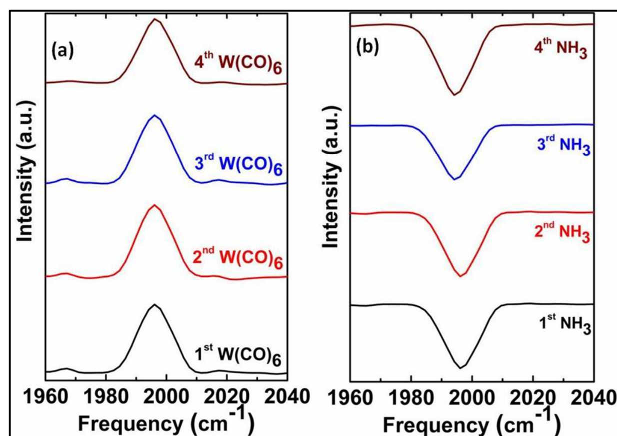

Fig. 3 Difference FTIR spectra of C=O stretch for four half cycles reaction (a) after W(CO)6 dosing and (b) after NH3 dosing.

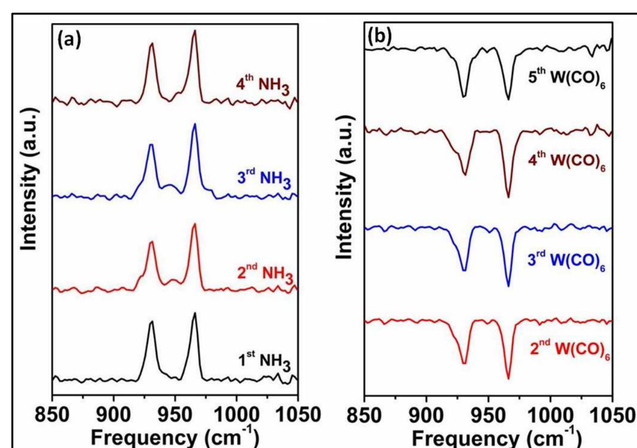

Fig. 4 Difference FTIR spectra of –NH2 twist for four half cycles reaction (a) after NH3 dosing and (b) after W(CO)6 dosing.

Figure 5a and 5b shows the characteristic peak of W4f and N1s respectively as obtained from X-ray photoelectron spectroscopy (XPS) in the as-deposited film of tungsten nitride grown on Si substrate. The complete survey in the binding energy range of 0-1000 eV also shows the presence of other electronic states of W (figure S1) and is in good agreement with the literature.[32] A negligible peak intensity corresponding to C1s electronic state confirms the negligible amount of C present (< 1 atomic %) in the as-grown film. However, a prominent peak at around 532 eV shows the presence of O in the film which may appear due to the oxide formation of the nitride film when exposed to the atmosphere prior to XPS measurements and or because of some chemisorbed hydroxyl species at the surface of the film. The spin orbital positions of 4f electron for W were observed at binding energies (BE) corresponding to 32.5 eV and 34.6 eV and 37.8 which reflects the W to be present in W_2N form in the as-deposited film.[33] While the two peaks at 32.5 eV and 34.6 eV are attributed to the W-N bond of W_2N,[34, 35] the peak at higher value of BE can be assigned to W 4f of W-O. The location of the $W4f_{7/2}$ at higher than W^0 (31.4 ± 0.2 eV) but slightly lower than the W^{+4}

Physical Chemistry Chemical Physics Accepted Manuscript

This journal is © The Royal Society of Chemistry 20xx

(32.8 ± 0.2 eV) further confirms the $W^{+\delta}$ state of the W in W_2N where $0 < \delta < 4$.[36] The BE difference of 2.1 eV further reflects the exact separation between these two spin of $W4f_{7/2}$ and $4f_{5/2}$ electrons.[36] The BE location of N1s electron at 397.1 eV is also in good agreement corresponding to nitride ion ($N^{-\delta}$) associated with W-N bond. The hump along with the N1s peak at 400.2 eV appeared due to the N atoms or molecules present at the interstitial sites of the W_2N. The presence of this interstitial N in W_2N film is common observation and well reported in literatures.[34, 37]Further quantitative analysis was carried out to determine the approximate ratio between W and N in the as-grown film. The normalized area under the individual XPS peaks for W and N are divided by their corresponding sensitivity factor and their ratio has been calculated. The atomic ratio of W to N thus comes out to be ca. 1.85:1.

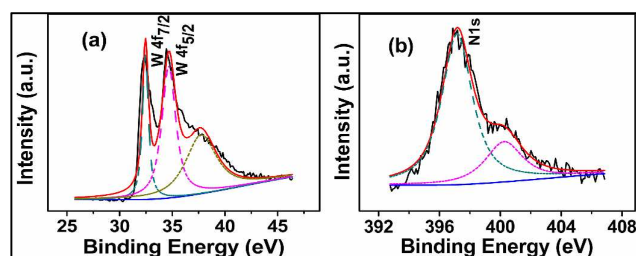

Fig. 5 XPS of the as deposited film showing peaks for (a) W4f5/2 and 4f7/2 electrons and (b) N1s electron.

The as-deposited film was found amorphous as shown in figure 6. X-ray diffraction (XRD) study and the selected area electron diffraction (SAED) pattern obtained from transmission electron microscopy did not show any diffraction peak or fringes. However, the films got converted to a crystalline phase once it was annealed under NH_3 atmosphere for one hour at 450 ^oC. The characteristic peaks of hexagonal-tungsten nitride (h-W_2N) were well matched with the JCPDS card no 01-075-0988 having the highest intense peak for h-W_2N at 11.45^o that corresponds to the (003) plane of the crystal. A set of parallel planes (004), (006) and (007) in addition to (003) indicates the growth of film in Z-axis of the crystal. Figure 6c and d show the field emission transmission spectroscopy (TEM) of the annealed films. The material from annealed film was scratched off followed by a sonication in iso-propyl alcohol for few minutes. The sample suspended in a very dilute form was then transferred to the TEM grid by casting few drops on it. The co-centric diffraction fringes in SAED pattern confirms the crystalline phase of the annealed film beyond further doubt. The different fringes are assigned to different planes of h-W_2N as calculated with their corresponding interplanner d-spacing matched with the same JCPDS card (01-075-0988) referred earlier in XRD. A family of parallel planes (003), (004), (005), (006) and (007) along Z-axis were eventually present in the SAED of obtained from the TEM that reflected few of the same planes found in the XRD of the same film. The high resolution TEM (HR-TEM) clearly shows the lattice array of the crystalline film (figure 6d). The *d*-spacing of 2.5 Å corresponds to the (008) plane of h-W_2N. A high-resolution TEM image shows a uniform film of WN_x grown on ZnO (figure S2a) that reflects the potential of ALD to deposit a conformal and highly uniform film. The RMS surface roughness of the as-deposited film was found to be as low as 0.5 nm over a 1 µm x 1 µm area determined by atomic force microscopy (AFM) (figure S2b). Such low roughness of the ALD grown film is another advantage to use it where a highly smooth surface is required.

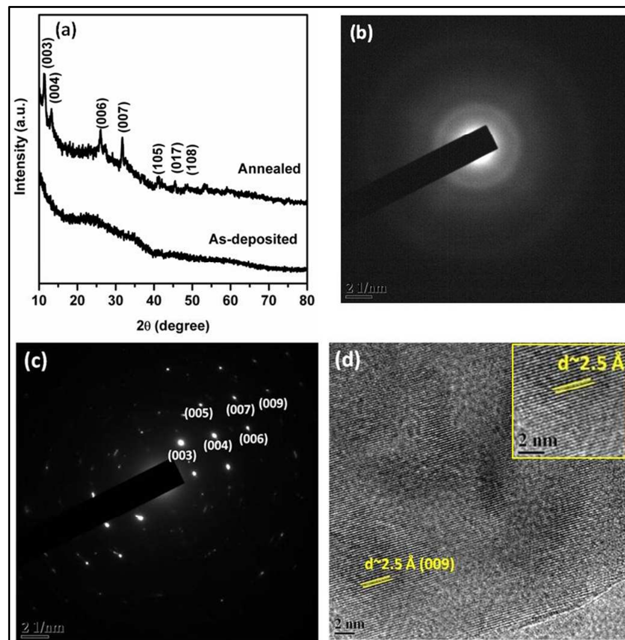

Fig. 6 (a) XRD pattern of the as deposited and the annealed film, (b) TEM-SAED of the as-deposited film, (c) SAED pattern and (d) HR-TEM image of the annealed h-W2N film (in inset a zoom view of the crystal lattice).

Electrical properties of the as deposited film was studied with a commercially available Hall measurement setup, under van der Paw configuration, to estimate the bulk carrier density and resistivity within temperature range of 80 K to 350 K. Film of ca. 40 nm thickness deposited on glass substrate was used for this measurement. Figure 7a shows the carrier concentration ($\#/cm^3$) plotted against increasing temperature (T) where T is in Kelvin. The carrier concentration at 80 K was found out to be 3×10^{18} cm^{-3} that increases exponentially and saturates beyond 180 K. The increase in carrier concentration is probably caused by the thermal generation of the carriers from the shallow trap states. Considerably high bulk carrier concentration of ca. 5-6 x 10^{20} cm^{-3} at room temperature (300 K) hinted at the metallic nature of the deposited film as also found from the ohmic nature of the current voltage plot. Resistivity of the same film is plotted against increasing T in figure 7b. It decreases with temperature as a well-known fact of thermal generations in semiconductor with increasing temperature. As mentioned earlier, the contribution for thermal generation mostly comes from the shallow states below the conduction band edge of the material.
The film resistivity at 80 K is as high as 3.2 Ω-cm that drops by more than ten times to ca. 0.3 Ω-cm at or beyond room

Physical Chemistry Chemical Physics Accepted Manuscript

Please do not adjust margins

temperature. For a n-type semiconductor the temperature dependence of the resistivity can be written as $\rho=\rho_0\exp -[(E_c-E_d)/kT]$ where ρ_0 and ρ are the resistivity at 0 K and T K respectively, E_c and E_d are the band positions of conduction band edge and donor level in the semiconductor and k is the Boltzman's constant. An Arrhenius plot between log (ρ) and 1/T is further drawn in the inset of figure 9a to estimate the activation energy [(E_c-E_d) or E_a].[38, 39] The slope obtained from this Arrhenius plot in the lower temperature regime (80-180 K) of the graph where the carrier concentration increases with temperature reflects the activation energy (E_a= 2.302*k*slope) of the material which comes out to be as low as 8 meV. Such a small value of activation energy complements the existence of shallow level electronic states just below the conduction band edge of the material and in turn reflects qualitatively the exponential increment of the carrier concentration with increasing temperature. Current-voltage measurement of the as-deposited film was performed to confirm the metallic behavior of the same as-grown W_2N film. Two Cu contacts were made on top the film by thermal evaporation. In the inset of figure 7a shows an I-V measurement in a range of -5V to +5V of the same film used for Hall measurement. The ohmic nature of the I-V measurement confirmed the metallic behavior of the deposited film beyond any further doubt.

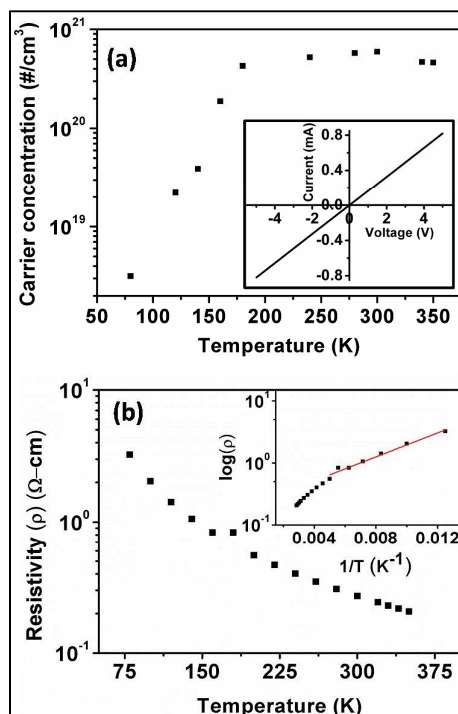

Fig. 7 (a) Carrier concentration as a function of increasing temperature (in inset I-V measurement at room temperature) and (b) resistivity as a function of increasing temperature (corresponding Arrhenius plot in inset) of an as-deposited film on glass substrate.

Electrochemical lithium storage property of as prepared WN_x film was studied as anode material similar to other transition metal nitrides. As WN_x possesses good electronic conductivity so it could be considered as a carbon and binder free electrode material for lithium-ion batteries. However, ALD used in the current work for preparing the film yields very low mass loading which in turn might affect the overall capacity of the cell. It leads us to think of a scaffold layer that can manifold the expose surface to deposit WN_x enabling us for more mass loading with the same numbers of ALD cycles. Multiwall carbon nanotube (MWCNT) was deposited by drop-cast method on SS coin on top of which WN_x was further deposited by ALD. Since, ALD process has high step-coverage property hence WN_x can easily be coated in a conformal way on MWCNT. The surface SEM views of the as deposited WN_x on bare SS substrate and the film on drop-cast CNT on SS substrate are shown in figure 8. A quantum increase of the surface for the deposit can clearly be understood from the figure depicted below. The phase confirmation of the WNx film was performed by XRD measurement (figure S3) and it showed the similar amorphous nature of the deposited film on MWCNT as well. However, we found a small peak corresponding to the (002) plane of CNT at around 26°.

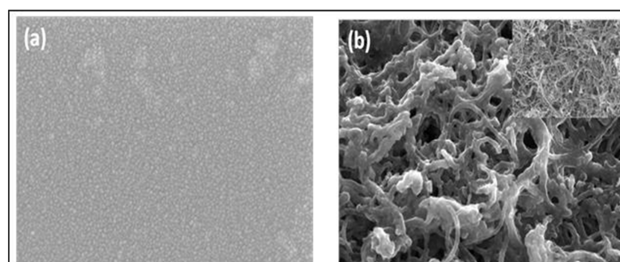

Fig. 8(a). Surface SEM of the as-deposited WNx film on SS substrate, (b) Surface SEM of the film deposited on drop-casted CNT (in inset the bare CNT on SS substrate).

A cyclic voltammetry (CV) study as well as charge-discharge performance of as-deposited WN_x film on SS substrate and on SS-MWCNT substrate are shown in figure 9. The CV profile in figure 9 (a) shows a prominent peak at 0.75 V during the cathodic process which can be ascribed to the conversion reaction between WN_x and Li to form Li_3N and W. During the reverse anodic process one broad peak at 1.4 V along with a small peak at 1.9 V was observed. The broad peak at 1.4 V can be de-convoluted into two peaks at 1.04 V and 1.4 V. In the consecutive cycles no changes were observed in the anodic peak position however during the cathodic process an extra peak at 1.4 V was appeared along with the peak at 0.75 V. After the 2nd cycle no changes has been observed in the peak position or in the peak intensities. Two cathodic peaks in the reduction process suggest that the reaction of WN_x with lithium is a multistep reaction, similarly the delithiation process also consist of two step delithiation process. Existing literature also supports the multistep lithiation and delithiation process for different nitride materials.[11, 14] CV of WN_x film on MWCNT was also performed under similar conditions as shown in figure 9(b). The CV profile (figure 9(b)) reflects a superposition of the bare WN_x electrode (figure 9(a)) and bare MWCNT electrode (figure S4). However, it slightly deviated from the CV of bare WN_x electrode. The cathodic peak at 1.4 V and the anodic peak at 1.9 V were disappeared

Physical Chemistry Chemical Physics Accepted Manuscript

 This journal is © The Royal Society of Chemistry 20xx

Please do not adjust margins

whereas as the cathodic peak at 0.75 V was moved to a higher potential of 0.95 V. Reason for such behavior is not known to us and subjected to some further studies. However the anodic peak positions were unchanged. The sharp peak in the regime of 0.2-0.1 V corresponds to the Li^+ intercalation in CNT (see the CV of MWCNT; figure S4) while the anodic peak at 0.13 V is due to the lithium removal from MWCNT. The charge discharge profiles (figure 9(c) and 9(d)) are also in good agreement with the CV profile. Two plateaus were observed during the discharge process at potential around 1.4 V and at 0.5 V vs. Li/Li^+ while an extended plateau at around 1.5 V was observed during the charge process.

A constant current charge-discharge performance of the WN_x film on SS and on MWCNT deposited SS substrate is shown in figure 9 (e). The as-prepared material shows a stable capacity almost from very beginning. A constant discharge capacity of ca. 5.5 µAh cm^{-2} was obtained for the material from 10 cycles onwards. A low discharge capacity per unit area was observed due to very low mass loading (ca. 100 µg in 1500 ALD cycles under saturation condition) in this case while an increase in the specific capacity was observed when MWCNT scaffold was used. As a result the discharge capacity of the cell was increased more than by four times to reach ca. 25 µAh cm^{-2}. The increased capacity was eventually contributed by both MWCNT as well as enhancement in the material loading due to the increase in effective surface area for depositing the active material. A comparison between the first two cycles of CVs for bare WN_x film and the film on MWCNT shows a clear increase in the overall capacity (figure S5). Though MWCNT takes part in electrochemical reaction against Li at a very low potential (0.1-0.2 V) contributing certain amount of capacity (around 9 µAh cm^{-2}; figure S6) but increase in the mass loading of WN_x is the major contributor to the capacity enhancement. The sharp fall in the discharge capacity for MWCNT-WN_x film in the second cycle is due the irreversible loss which is mostly caused by the SEI formation. Similar observation was also noticed in the cycling performance of bare MWCNT film (figure S6) and the SEI formation was evident from the CV of the same (figure S4). In a nutshell, this study primarily shows the advantage of using the drop-casted MWCNT for enhancing the surface area for the deposit leading to an increase in the overall capacity of the cell. However, the coulombic efficiency calculated for both the cases came out to be more than 99% (figure 9f) that is highly stable till 200 cycles. Such high coulombic efficiency was obtained for WN_x thin films electrode due to its high electronic conductivity which was observed in Hall measurements and discussed earlier. It is well demonstrated in the earlier literature that conductivity of the electrode has a positive impact on the coulombic efficiency. Thus the preliminary tests of the as-deposited WN_x films as an anode material in Li-ion battery opens up a new possibility for future research. The incorporation of high surface area MWCNT facilitates the performance of the anode to a good extent.

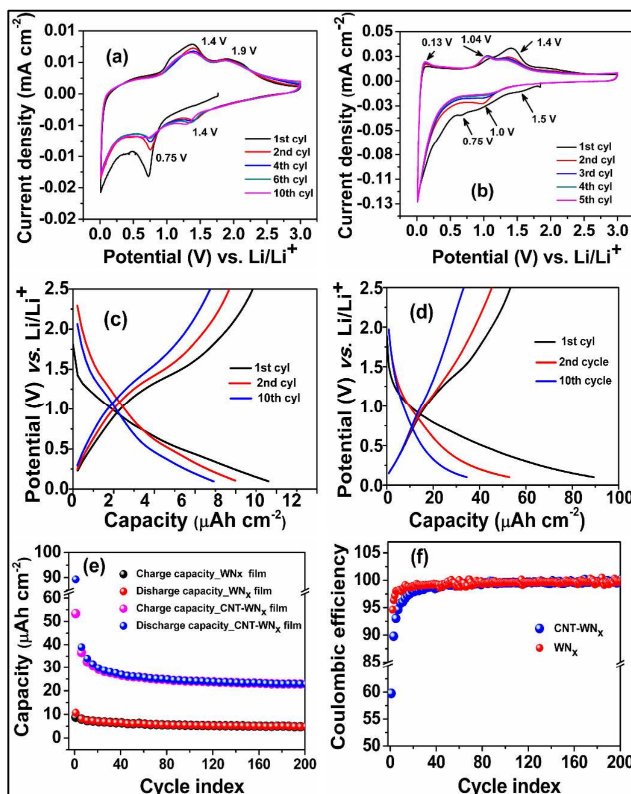

Fig. 9 CV of the as-deposited WNx film (a) and WN_x@CNT film (b); charge/discharge profiles of bare WN_x (c) and WNx@CNT (d) in the 1st, 2nd and 10th cycles; The cycling performance of both these films for 200 cycles (e) and Coulombic efficiencies of the films as calculated from their respective cycling performances (f).

To predict the reaction mechanism of as-grown film with Li under operation, an intensive *ex-situ* XRD analysis was performed and shown in figure 10. XRD was carried out on the WN_x film on SS substrate, before cycling, after first discharge (at 0.1 V *vs*. Li/Li^+) and after first charge (3.0 V *vs*. Li/Li^+) process. As shown in the XRD of SS and the as-grown film on the SS before cycling, we did not observe any extra peak except the three prominent peak at 43.6, 50.7 and 74.5^o all of which can perfectly be assigned to the stainless steel substrate. The absence of any signature peak for the as-grown tungsten nitride film is thus in complete agreement with the earlier analysis and reconfirmed the film to be amorphous in nature. However, four new peaks have been recorded for the WN_X electrode after discharged up to 0.01 V *vs.* Li/Li^+. The peak at 32.6^o can be ascribed to the (101) plane for Li_3N or (101) plane for LiOH (JCPDS card no. 01-078-2005 and 01-085-0736 respectively). The other peak at 24.8^o can be assigned to the W (110) plane or WO_3 (200) (JCPDS card no. 03-065-6453 and 01-075-2072 respectively). However, here we prefer to assign the peak to WO_3 as the peak corresponds W at this 2θ possess very low intensity and the prominent peaks correspond to metallic W are mostly located at or beyond 40°. One more peak at 21.5^o corresponds to the (020) plane of $LiOH(H_2O)$ was also observed after the discharge cycle (visible in the enlarged view of the XRD in figure 10(b). The presence of Li_3N and or LiOH as well as WO_3 in the film after discharging

Physical Chemistry Chemical Physics Accepted Manuscript

Please do not adjust margins

the cell confirms the conversion based reaction of the WN_x in Li-ion battery. The presence of LiOH and WO_3 peaks in the cell after discharge process could be due to the reaction of Li_3N and W with atmospheric moisture (H_2O) while exposed in air during sample loading for XRD measurements. It is an obvious fact that Li_3N readily reacts with H_2O and form LiOH and NH_3. Similar observation was reported earlier where Zn_3N_2 was used as an anode in Li-ion battery.[40] On the contrary, all these signature peaks disappeared when the cell was fully charged which clearly indicates the re-conversion of Li_3N to Li and WN_x. However, the peak at 21.3^o remains unaltered even after the complete charge cycle. It could be due to the presence of Li_2CO_3 and the plane correspond to 21.3^o can perfectly be assigned to the (110) plane of the monoclinic-Li_2CO_3 (JCPDS card no. 01-083-1454). The presence of this peak in both after discharge and charge cycle can easily be explained by the formation of Li_2CO_3 [as a component of solid electrolyte layer (SEI)] due to electrolyte decomposition.[41, 42]

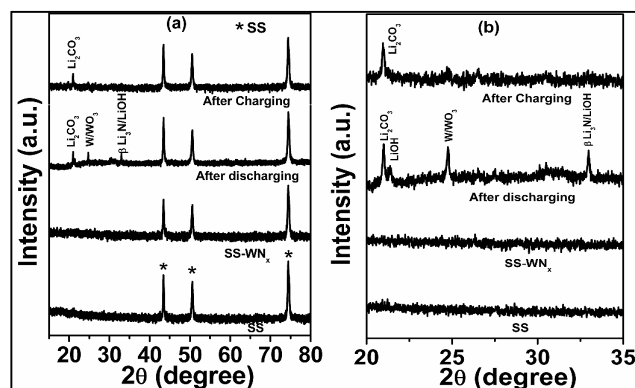

Fig. 10 (a) XRD of the SS and the film on SS before cycling, after first complete discharge and after charge cycle and (b) an enlarged view of the same.

Conclusions

Tungsten nitride is successfully grown by ALD within a narrow temperature window between 180-195°C using tungsten hexacarbonyl and ammonia as precursors. A saturated growth rate of ca. 0.35 Å per ALD cycle was observed with the help of QCM, ellipsometry and XRR measurements. *In-situ* FTIR study confirmed the surface species after each half reaction and enabled us to predict the possible reaction mechanism associated with the ALD of tungsten nitride. XPS confirmed the presence of W_2N phase in the film. The XRD and HR-TEM depicted the as-deposited film to be amorphous which got converted to h-W_2N upon annealing at an elevated temperature under NH_3 atmosphere. Hall and current-voltage measurement of the as-deposited film showed the grown film to be highly conducting due to the presence of shallow donor levels. The electrochemical studies of the as-deposited WN_x films showed the potential for using it as a stable anode material for Li-ion battery with a high coulombic efficiency more than 99 % even up to 200 cycles. The conversion based reaction mechanism for WN_x with Li was also confirmed with an *ex-situ* XRD analysis.

Acknowledgements

This work was supported by the National Centre for Photovoltaic Research and Education funded by the Ministry of New and Renewable Energy, Govt. of India. The authors acknowledge the Dept. of Physics and SAIF IIT Bombay for the AFM and TEM facility.

Notes and references

‡Footnotes relating to the main text should appear here. These might include comments relevant to but not central to the matter under discussion, limited experimental and spectral data, and crystallographic data.

§

§§

etc.

1 K. R.McClain, C.O'Donohue, A.Koley, R. O.Bonsu, K. A.Abboud, J. C.Revelli, T. J. Anderson and L.McElwee-White, *J. Am. Chem. Soc.* 2014,**136**, 1650-1662.
2 D.Kim, O. H.Kim,T.Anderson, J.Koller, L.McElwee-White, L.-C.Leu, J. M. Tsai and D. P.Norton, *J. Vac. Sci. Technol. A* 2009,**27,** 943-950.
3 M. G.Sung, K.-Y.Lim, H.-J.Cho, S. R.Lee, S.-A.Jang, Y. S.Kim, T.-Y.Kim, H.-S.Yang, J.-C. Ku and J. W.Kim, *Jpn. J Appl. Phys. 1* 2007,**46,** 7256-7262.
4 Z. W.Li, R. G.Gordon, D. B.Farmer, Y. B. Lin and J.Vlassak, *Electrochem. Solid State Lett.* 2005,**8,** G182-G185.
5 W.-F.Chen, J. T. Muckerman and E.Fujita, *Chem. Comm.* 2013,**49,** 8896-8909.
6 M.-S.Balogun, W.Qiu, W.Wang, P.Fang, X.Lu and Y.Tong, *J. Mater. Chem. A* 2015,**3,** 1364-1387.
7 M. Chhowalla and H. E.Unalan, *Nat. Mater.* 2005,**4,** 317-322.
8 H.Zhong, H.Zhang, Y.Liang, J.Zhang, M. Wang and X.Wang, *J. Power Sources* 2007,**164,** 572-577.
9 D.Choi and P. N.Kumta, *J. Am. Ceram. Soc.* 2007,**90,** 3113-3120.
10 A. R.Ko, S.-B.Han, Y.-W. Lee and K.-W.Park, *Phys. Chem. Chem. Phys.* 2011,**13,** 12705-12707.
11 Q. Sun and Z.-W.Fu, *Electrochim. Acta* 2008,**54,** 403-409.
12 K.Zhang, H.Wang, X.He, Z.Liu, L.Wang, L.Gu, H.Xu, P.Han, S.Dong, C.Zhang, J.Yao, G.Cui and L.Chen, *J. Mater. Chem.* 2011,**21,** 11916-11922.
13 Y.Yue, P.Han, X.He, K.Zhang, Z.Liu, C.Zhang, S.Dong, L. Gu and G.Cui, *J. Mater. Chem.* 2012,**22,** 4938-4943.
14 B.Das, M. V.Reddy, G. V. S. Rao and B. V. R.Chowdari, *J. Mater. Chem.* 2012,**22,** 17505-17510.
15 B.Das, M. V.Reddy, G. V. S. Rao and B. V. R.Chowdari, *RSC Adv.* 2012,**2,** 9022-9028.
16 D. K.Nandi, U. K.Sen, D.Choudhury, S. Mitra and S. K.Sarkar, *ACS Appl. Mater. Interfaces* 2014,**6,** 6606-6615.
17 S.Wang, X.Yu, Z.Lin, R.Zhang, D.He, J.Qin, J.Zhu, J.Han, L.Wang, H.-k.Mao, J.Zhang and Y.Zhao, *Chem. Mater.* 2012,*24*, 3023-3028.
18 Marchand, R., Tessier, F. and DiSalvo, F. J., *J. Mater. Chem.* 1999,**9,** 297-304.
19 M. H.Tsai, S. C.Sun, H. T. Chiu and S. H.Chuang, *Appl. Phys. Lett.* 1996,**68,** 1412-1414.
20 J. E.Kelsey, C.Goldberg, G.Nuesca, G.Peterson, A. E.Kaloyeros and B.Arkles, *J. Vac. Sci. Technol. B* 1999,**17,** 1101-1104.
21 G.Soto, W.de la Cruz, F. F.Castillon, J. A.Diaz, R.Machorro and M. H.Farias, *Appl. Surf. Sci.* 2003,**214,** 58-67.

Physical Chemistry Chemical Physics Accepted Manuscript

This journal is © The Royal Society of Chemistry 20xx

Please do not adjust margins

22 M.Bereznai, Z.Toth, A. P.Caricato, M.Fernandez, A.Luches, G.Majni, P.Mengucci, P. M.Nagy, A. Juhasz and L.Nanai, *Thin Solid Films* 2005,**473,** 16-23.
23 J. W.Klaus, S. J. Ferro and S. M.George, *Appl. Surf. Sci.* 2000,**162,** 479-491.
24 H. S.Sim, S. I. Kim and Y. T.Kim, *J. Vac. Sci. Technol. B* 2003,**21,** 1411-1414.
25 S.-H.Kim, J.-K.Kim, J. H.Lee, N.Kwak, J.Kim, S.-H.Jung, M.-R.Hong, S. H.Lee, J. Collins and H.Sohn, *J. Electrochem. Soc.* 2007,**154,** D435-D441.
26 J. S. Beckerand R. G. Gordon, *Appl. Phys. Lett.* **2003,***82*, 2239-2241.
27 J.Malm, T. Sajavaara and M.Karppinen, *Chem. Vapor Depos.* 2012,**18,** 245-248.
28 M.Diskus, O. Nilsen and H.Fjellvag, *J. Mater. Chem.* 2011,**21,** 705-710.
29 M.Diskus, M.Balasundaram, O. Nilsen and H.Fjellvag, *Dalton Trans.* 2012,**41,** 2439-2444.
30 D. K.Nandi, U. K.Sen, D.Choudhury, S. Mitra and S. K.Sarkar, *Electrochim. Acta* 2014,**146**, 706-713.
31 M.Broquier, C.Crépin, H. Dubost and J. P.Galaup, *Chem. Phys.* 2007,**341,** 207-217.
32 Y. M.Zhao, W. B.Hu, Y. D.Xia, E. F.Smith, Y. Q.Zhu, C. W.Dunnill and D. H.Gregory, *J. Mater. Chem.* 2007,**17,** 4436-4440.
33 Y. G.Shen, Y. W.Mai, W. E.McBride, Q. C. Zhang and D. R.McKenzie, *Thin Solid Films* 2000,**372,** 257-264.
34 Y. G. Shen and Y. W.Mai, *Surf. Coat. Technol.* 2000,**127,** 238-245.
35 M.Nagai, T.Suda, K.Oshikawa, N. Hirano and S.Omi, *Catal. Today* 1999,**50,** 29-37.
36 C.Shi, X. F.Yang, A. M. Zhu and C. T.Au, *Catal. Today* 2004,**93–95,** 819-826.
37 M. Nagai and K.Kishida, *Appl. Surf. Sci* 1993,**70–71***, Part 2*, 759-762.
38 R.Wan, M.Yang, Q. Zhou and Q.Zhang, *J. Vac. Sci. Technol. A* 2012,**30**.
39 K. Agilandeswari and A. R.Kumar, *J. Magn. Magn. Mater.* 2014,**364,** 117-124.
40 N.Pereira, L. C. Klein and G. G.Amatucci, *J. Electrochem. Soc.* 2002,**149,** A262-A271.
41 K.Tasaki, A.Goldberg, J.-J.Lian, M.Walker, A. Timmons and S. J.Harris, *J. Electrochem. Soc.* 2009,**156,** A1019-A1027.
42 E.Peled, C.Menachem, D. BarTow and A.Melman, *J. Electrochem. Soc.* 1996,**143,** L4-L7.

Physical Chemistry Chemical Physics Accepted Manuscript

Please do not adjust margins